

TeV GAMMA-RAY OBSERVATIONS OF THE PERSEUS AND ABELL 2029 GALAXY CLUSTERS

J. S. PERKINS,¹ H. M. BADRAN,² G. BLAYLOCK,³ S. M. BRADBURY,⁴ P. COGAN,⁵ Y. C. K. CHOW,⁶ W. CUI,⁷ M. K. DANIEL,⁵
 A. D. FALCONE,⁸ S. J. FEGAN,⁶ J. P. FINLEY,⁷ P. FORTIN,⁹ L. F. FORTSON,¹⁰ G. H. GILLANDERS,¹¹ K. J. GUTIERREZ,¹
 J. GRUBE,⁴ J. HALL,¹² D. HANNA,¹³ J. HOLDER,⁴ D. HORAN,¹⁴ S. B. HUGHES,¹ T. B. HUMENSKY,¹⁵ G. E. KENNY,¹¹
 M. KERTZMAN,¹⁶ D. B. KIEDA,¹² J. KILDEA,¹³ K. KOSACK,¹ H. KRAWCZYNSKI,¹ F. KRENNRICH,¹⁷ M. J. LANG,¹¹
 S. LEBOHEC,¹² G. MAIER,⁴ P. MORIARTY,¹⁸ R. A. ONG,⁶ M. POHL,¹⁷ K. RAGAN,¹³ P. F. REBILLLOT,¹
 G. H. SEMBROSKI,⁷ D. STEELE,¹⁰ S. P. SWORDY,¹⁹ L. VALCARCEL,¹³ V. V. VASSILIEV,⁶
 S. P. WAKELY,¹⁹ T. C. WEEKES,¹⁴ AND D. A. WILLIAMS²⁰
 (THE VERITAS COLLABORATION)

Received 2005 November 9; accepted 2006 February 10

ABSTRACT

Galaxy clusters might be sources of TeV gamma rays emitted by high-energy protons and electrons accelerated by large-scale structure formation shocks, galactic winds, or active galactic nuclei. Furthermore, gamma rays may be produced in dark matter particle annihilation processes at the cluster cores. We report on observations of the galaxy clusters Perseus and A2029 using the 10 m Whipple Cerenkov telescope during the 2003–2004 and 2004–2005 observing seasons. We apply a two-dimensional analysis technique to scrutinize the clusters for TeV emission. In this paper we first determine flux upper limits on TeV gamma-ray emission from point sources within the clusters. Second, we derive upper limits on the extended cluster emission. We subsequently compare the flux upper limits with EGRET upper limits at 100 MeV and theoretical models. Assuming that the gamma-ray surface brightness profile mimics that of the thermal X-ray emission and that the spectrum of cluster cosmic rays extends all the way from thermal energies to multi-TeV energies with a differential spectral index of -2.1 , our results imply that the cosmic-ray proton energy density is less than 7.9% of the thermal energy density for the Perseus Cluster.

Subject headings: galaxies: clusters: general — galaxies: individual (NGC 1275) —
 galaxies: clusters: individual (Abell 426, Perseus, Abell 2029) — gamma rays: observations

1. INTRODUCTION

As our universe evolves and structure forms on increasingly larger scales, the gravitational energy of matter is constantly converted into random kinetic energy of cosmic gas. In galaxy clusters, collisionless structure formation shocks are thought to be the main agents responsible for heating the intercluster medium (ICM) to temperatures of $k_B T \simeq 10$ keV. Through this and other processes, gravitational energy is converted into the random kinetic energy of nonthermal baryons (protons) and leptons (electrons). Galactic winds (Völk & Atoyan 1999) and reacceleration of mildly relativistic particles injected into the ICM by powerful cluster members (Enßlin & Biermann 1998) may accelerate additional particles to nonthermal energies. Using Galactic cosmic rays (CRs) as a yard stick, one expects that the energy density of cosmic-ray protons (CRPs) dominates over that of cosmic-ray electrons (CREs) by approximately 2 orders of magnitude and may be comparable to that of thermal particles and the ICM mag-

netic field. CRPs can diffusively escape clusters only on timescales much longer than the Hubble time. Therefore, they accumulate over the entire formation history (Völk & Atoyan 1999). CREs lose their energy by emitting synchrotron, bremsstrahlung, and inverse Compton emission on much shorter timescales. For ICM magnetic fields on the order of $B \simeq 1$ μ G, synchrotron and inverse Compton emission losses alone cool CREs of energy $E = 1$ TeV on a timescale

$$\tau_s = \left(\frac{4}{3} \sigma_T c \frac{B'^2}{8\pi m_e c^2} \gamma_e \right)^{-1}, \quad (1)$$

where σ_T is the Thomson cross section, $B' = (B^2 + B_{\text{CMB}}^2)^{1/2}$, and $B_{\text{CMB}} = 3.25(1+z)^2$ μ G; for the clusters considered here, $z \ll 1$ and $\tau_s \approx 10^6$ yr.

There is good observational evidence of nonthermal electrons in galaxy clusters. For a number of clusters, diffuse synchrotron radio halos and/or radio relic sources have been detected (Giovannini et al. 1993, 1999; Giovannini & Feretti 2000;

¹ Department of Physics, Washington University in St. Louis, St. Louis, MO 63130.

² Physics Department, Tanta University, Tanta, Egypt.

³ Department of Physics, University of Massachusetts, Amherst, MA 01003-4525.

⁴ School of Physics and Astronomy, University of Leeds, Leeds LS2 9JT, UK.

⁵ School of Physics, University College Dublin, Belfield, Dublin 4, Ireland.

⁶ Department of Physics and Astronomy, University of California, Los Angeles, CA 90095.

⁷ Department of Physics, Purdue University, West Lafayette, IN 47907.

⁸ Department of Astronomy and Astrophysics, Penn State University, University Park, PA 16802.

⁹ Department of Physics and Astronomy, Barnard College, Columbia University, NY 10027.

¹⁰ Astronomy Department, Adler Planetarium and Astronomy Museum, Chicago, IL 60605.

¹¹ Physics Department, National University of Ireland, Galway, Ireland.

¹² Physics Department, University of Utah, Salt Lake City, UT 84112.

¹³ Physics Department, McGill University, Montreal, QC H3A 2T8, Canada.

¹⁴ Fred Lawrence Whipple Observatory, Harvard-Smithsonian Center for Astrophysics, Amado, AZ 85645.

¹⁵ Enrico Fermi Institute, University of Chicago, Chicago, IL 60637.

¹⁶ Department of Physics and Astronomy, DePauw University, Greencastle, IN 46135-0037.

¹⁷ Department of Physics and Astronomy, Iowa State University, Ames, IA 50011.

¹⁸ Department of Physical and Life Sciences, Galway-Mayo Institute of Technology, Dublin Road, Galway, Ireland.

¹⁹ Enrico Fermi Institute, University of Chicago, Chicago, IL 60637.

²⁰ Santa Cruz Institute for Particle Physics and Department of Physics, University of California, Santa Cruz, CA 95064.

Kempner & Sarazin 2001; Feretti 2003). For some clusters, an excess of extreme ultraviolet (EUV) and/or hard X-ray radiation over that expected from the thermal X-ray-emitting ICM has been observed (Bowyer & Berghöfer 1998; Lieu et al. 1999; Rephaeli et al. 1999; Fusco-Femiano et al. 2004). The excess radiation originates most likely as inverse Compton emission from CRE scattering cosmic microwave background photons (Lieu et al. 1996; Enßlin & Biermann 1998; Blasi & Colafrancesco 1999; Fusco-Femiano et al. 1999).

The detection of gamma-ray emission from galaxy clusters would make it possible to measure the energy density of nonthermal particles. The density and energy density of the thermal ICM can be derived from imaging-spectroscopy observations made with such satellites as *Chandra* and *XMM-Newton* (Krawczynski 2002; Markevitch et al. 1998; Donahue et al. 2004). The density and energy spectra of the nonthermal protons could be computed from the detected gamma-ray emission once the density of the thermal ICM is known (Pfrommer & Enßlin 2004). Gamma rays can originate as inverse Compton and bremsstrahlung emission from CREs and as $\pi^0 \rightarrow \gamma\gamma$ emission from hadronic interactions of CRPs with thermal target material. If successful measurements of the gamma-ray fluxes from several galaxy clusters were obtained, one could explore the correlation of the CRP luminosity with cluster mass, temperature, and redshift, and draw conclusions about how the clusters grew to their observed size. If CRPs indeed contribute noticeably to the pressure of the ICM, the measurements of the CRP energy density would allow improvement on the estimates of the cluster mass based on X-ray data and thus improve estimates of the universal baryon fraction. If CR provide pressure support to the ICM, they would inhibit star formation to some extent as they do not cool radiatively like the thermal X-ray-emitting gas. Furthermore, low-energy CR ions might provide a source of heating the thermal gas (Rephaeli 1977).

In addition to a CR origin, annihilating dark matter may also emit gamma rays. The intensity of the radiation depends on the nature of dark matter, the annihilation cross sections, and the dark matter density profile close to the core of the cluster (e.g., Bergström et al. 1998). While MeV observations are ideally suited for detecting the emission from the bulk of the nonthermal particles, TeV gamma-ray observations of cluster energy spectra and radial emission profiles would allow us to disentangle the various components that contribute to the emission.

At MeV energies, various authors have searched for cluster emission based on the data from the EGRET detector on board the *Compton Gamma Ray Observatory*. Three studies revealed evidence at a significance level of approximately 3 standard deviations: Colafrancesco (2001) and Kawasaki & Totani (2002) reported an association between Abell clusters and unidentified gamma-ray point sources from the third catalog of the EGRET experiment; Scharf & Mukherjee (2002) found gamma-ray emission from Abell clusters by stacking the EGRET data of 447 galaxy clusters. However, analyzing the data from 58 galaxy clusters, Reimer et al. (2003) do not confirm a detection and give an upper limit that is inconsistent with the mean flux reported by Scharf & Mukherjee (2002). In the TeV energy range, Fegan et al. (2005) reported marginal evidence for emission from A1758 in the field of view of 3EG J1337 +5029.

In this paper we report on a search for TeV gamma-ray emission from the Perseus and Abell 2029 galaxy clusters with the Whipple 10 m Cerenkov telescope. We selected both clusters based on their proximity and high masses: Perseus ($z = 0.0179$) is at a distance of 75 Mpc from us and has a total mass of $4 \times 10^{14} M_{\odot}$; Abell 2029 ($z = 0.0775$) is 300 Mpc away from us, and its total mass has been estimated to be $5 \times 10^{14} M_{\odot}$ (Girardi et al. 1998).

The search described below assumes that the high-energy (HE) surface brightness mimics the X-ray surface brightness and focuses on the detection of gamma rays from within 0.8 from the cluster center. There are several possibilities relating the thermal and nonthermal particles within clusters. From general considerations, Völk & Atoyan (1999) assume that the nonthermal particles carry a certain fraction of the energy density of the ICM. One of the aims of very high energy (VHE) astronomy is to constrain this fraction. Indeed, we do know the CRP energy density in the interstellar medium (ISM) of the Milky Way. In this case it turns out that the CRP energy density is comparable to the energy density of the thermal ISM, the energy density of the interstellar magnetic field, and the energy density of starlight. If nonthermal particles in clusters indeed carry a certain fraction of the energy density of the ICM, the HE surface brightness would mimic that of the thermal X-ray emission. In another line of argument, one may assume that powerful cluster members (i.e., radio sources) are the dominant source of nonthermal particles in the ICM; also in this case we would expect that CRPs accumulate at the cluster cores where usually the most powerful radio galaxies are found (Pfrommer & Enßlin 2004). Ryu et al. (2003) and Kang & Jones (2005) performed numerical calculations to estimate the energy density of CRPs by large-scale structure formation shocks. The simulations indicate that strong shocks form preferentially in the cluster periphery. Accordingly, most CRPs would be accelerated in the outskirts of the clusters and would only slowly be transported to the cluster core by bulk plasma motion (e.g., following cluster merger). The main conclusion of this discussion is that the CRP distribution in galaxy clusters is uncertain as long as we have not mapped them in the light of HE photons. However, independent of the lateral profile of CRP acceleration, we expect that the emission profile will be centrally peaked, as the HE emission results from inelastic collisions of the CRPs with the centrally peaked thermal target material.

The sensitivity of the Whipple 10 m telescopes drops for angular distances exceeding 0.8 from the center of the field of view. For the Perseus Cluster, the temperature map of Churazov et al. (2003) shows a high-temperature region at about 0.25 from the cluster center. As the high-temperature region might be associated with shocks, this region might emit VHE emission. Our search for VHE emission does cover this region with high sensitivity. However, we did not perform a specialized search for merger-related emission.

In the case of the more distant cluster Abell 2029, our search region of 0.8 radius covers a physical region of 4.2 Mpc radius. Thus, our search includes all the cluster emission, independent of where in the cluster it originates.

The rest of the paper is organized as follows: we describe the Whipple 10 m telescope, the observations, data cleaning procedures, and the data analysis methods in § 2. The main results of this study are a search for point source emission from localized sources in the clusters and a search for diffuse emission from the ICM. We present these results in § 3 and discuss them in § 4. Reported uncertainties are 1 standard deviation, and upper limits are given at the 90% confidence level, unless otherwise stated. In the rest of the paper, we assume Hubble's constant $H_0 = 70 \text{ km s}^{-1} \text{ Mpc}^{-1}$, the dark energy density $\Omega_{\Lambda} = 0.7$, and the total matter density $\Omega_M = 0.3$.

2. DATA AND ANALYSIS

2.1. Instrumentation and Data Sets

TeV observations were taken on clear moonless nights with the Whipple 10 m Cerenkov telescope located on Mount Hopkins,

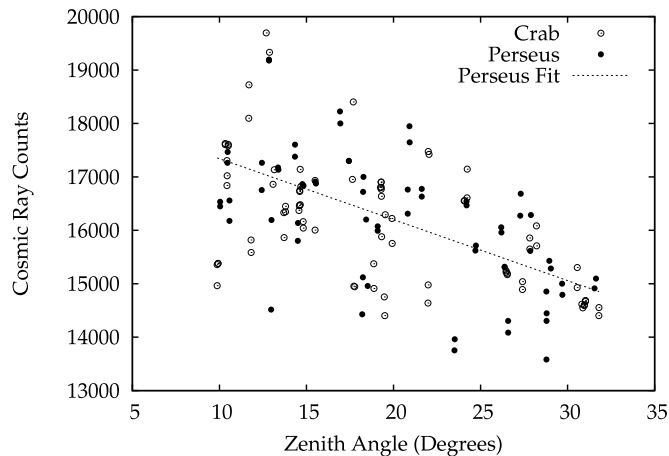


FIG. 1.—Cosmic-ray counts on a run-by-run basis vs. zenith angle. Shown are data from the Crab Nebula (*open circles*) and the Perseus Cluster (*filled circles*). We fitted each group of data (see the Perseus fit line for an example) to show the dependence of the rate on the zenith angle and rejected any runs that deviated by more than 10%.

Arizona, at an altitude of 2300 m above sea level. This telescope detects high-energy photons by imaging the flashes of Cerenkov light emitted by secondary particles in gamma-ray-induced air showers. The Whipple 10 m segmented mirror focuses the faint UV/blue Cerenkov flashes onto a camera consisting of photo-multiplier tube pixels. The Whipple telescope, including the current camera, has been described elsewhere (Finley et al. 2001).

We observed the Perseus Cluster between 2004 August 16 and 2005 February 5 (UT). Data were taken as pairs of 28 minute runs. An “ON” run pointed at the source was followed by an “OFF” run at the same azimuth and elevation but offset $7^{\circ}50'$ (30 minutes) in right ascension for background subtraction. Removing runs with low raw rates (indicative of poor sky conditions) and mismatched ON/OFF pairs (indicative of differing sky conditions between ON and OFF runs) resulted in 29 ON/OFF pairs for analysis. The cluster Abell 2029 was observed between 2003 March 7 and May 5 (UT) resulting in 14 ON/OFF pairs. A number of observations of the Crab Nebula (a “standard candle” in TeV gamma-ray astronomy) were taken to determine the detection efficiency and angular resolution for various points on the camera. Figure 1 illustrates the cosmic-ray rates of each run versus the zenith angle for both the Perseus and Crab observations. In this analysis, we only use those runs that deviate by less than 10% from the expected rate. Table 1 details the duration and observing season of the various data sets.

2.2. Standard Analysis

The data were analyzed using the standard second-moment-parameterization technique (Hillas 1985). We identify gamma-ray events and suppress background cosmic-ray events by applying gamma-ray selection criteria (EZCuts2004; see Kosack 2005), designed to be independent of zenith angle and energy and well suited for the analysis of extended sources. The two-dimensional arrival direction of each gamma-ray event was calculated from the orientation and elongation of the Cerenkov light distribution in the camera (Buckley et al. 1998). We estimate that the mean energy threshold for the Whipple 10 m to be approximately 400 GeV (Finley et al. 2001). More detailed descriptions of Whipple observing modes and analysis procedures have been given by Weekes (1996), Punch & Fegan (1991), and Reynolds et al. (1993).

TABLE 1
DESCRIPTION OF THE VARIOUS DATA SETS USED IN THIS ANALYSIS

Source	Season (MJD)	Number (pairs)	ON (min)	OFF (min)
Perseus	2004–2005	29	810.4	810.4
Abell 2029	2003–2004	13	363.3	363.3
Crab	2003–2004	29	810.4	810.4
Crab	2004–2005	24	670.7	670.4
Crab-0.5	2003–2005	6	167.7	167.6
Crab-0.8	2003–2005	8	223.6	223.6

NOTE.—The Crab sets titled “Crab-0.5” and “Crab-0.8” are observations performed with the telescope offset from the location of the Crab Nebula by $0^{\circ}5$ and $0^{\circ}8$, respectively.

2.3. Cluster-specific Analysis

In this section we describe the specific analysis techniques applied to the clusters, including the method used to search for point sources within each cluster. On the basis of the expected lateral emission profiles, we then discuss the examination of the cluster for diffuse emission.

In order to search for point sources within the field of view, the resolution and detection efficiency need to be known to good accuracy at all locations on the camera. Every search for extended emission should be preceded by a search for point sources. If there are point sources, the corresponding sky regions should be excluded from the search for extended emission. We used an empirical method based on data from the Crab Nebula that were taken during the same months as the Perseus and Abell 2029 data. The background-subtracted Crab data were binned by the square of the distance of the reconstructed shower direction from the location of the Crab Nebula (so as to eliminate any solid angle dependence) and fitted with an exponential. These fits gave us a direct measurement of the resolution of the camera for a point source at different locations within the field of view. From these same data we determined an optimal angular cut based on the integral number of excess and background counts as a function of angular distance from the source location. By calculating the gamma-ray rate at the different offsets, we also determined how the efficiency of the camera falls off toward the edges. This empirical

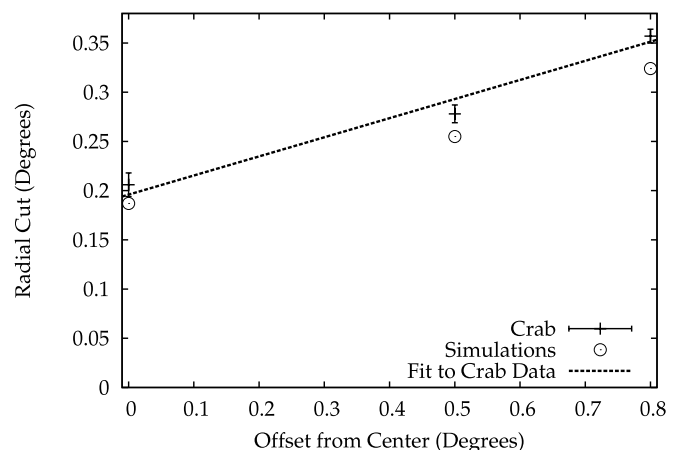


FIG. 2.—Optimal angular cut for different source locations on the camera. All the cuts accept $\sim 50\%$ of all the triggered Crab events. Shown are the results from the Crab observations in 2004 (*crosses*) and from Monte Carlo simulations (*circles*). The cut increases farther from the center due to the loss in resolution. The fit to the Crab data (*dashed line*) was used to search for point sources in the field of view.

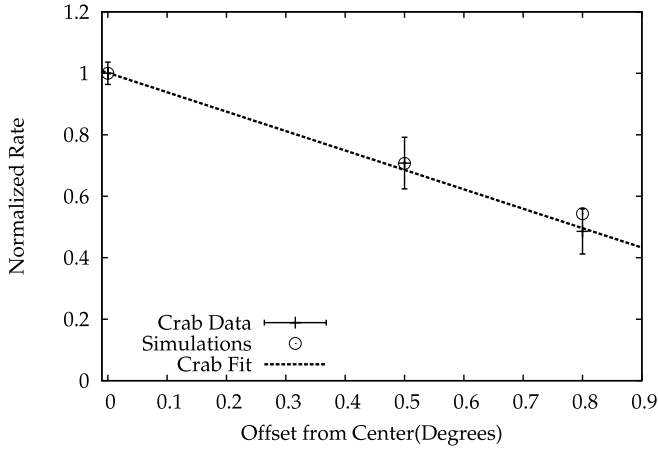


FIG. 3.—Crab gamma-ray rate normalized to 1.0 at zero offset (*crosses*) vs. offset from the center of the camera using the optimized cut found in Fig. 2. The fit to these data (*dashed line*) was used to calculate the upper limit for point sources within the field of view. Also shown are the results from Monte Carlo simulations (*circles*) that match the observational data very well. At the center of the field of view, the detection rate is 1.9 events per minute.

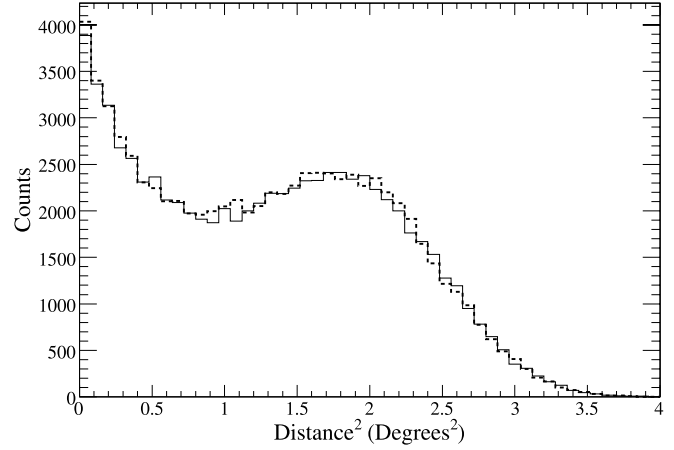


FIG. 4.—Number of Whipple 10 m Perseus observation events vs. the distance of the estimated arrival direction from the center of the field of view squared. The dashed line shows the OFF counts and the solid line the ON counts. There is a good match between the ON and the OFF data out to the edge of the camera, and no excess from the cluster is detected.

method was compared to Monte Carlo simulations of centered and offset data. The Monte Carlo code²¹ simulates atmospheric Cerenkov showers and calculates the response of the Whipple detector. The simulated data have the same format as the experimental data and were analyzed using the same methods as those applied to the real data. We produced a simulated shower set with a differential spectral index of -2.5 and fed this through the detector simulations for different source offsets and compared this with observations. Figure 2 shows the optimal angular cut at the three different offsets. The optimal cut was used to determine the total number of events originating from a specific point in the field of view. This cut increases from 0.2° at the camera center to 0.35° at a 0.8° source offset due to the poorer angular resolution toward the camera edge. Figure 3 shows the normalized gamma-ray rate for the source located at the various offsets using the cut from Figure 2. Compared to the center of the field of view, the rate decreases by 40% at 0.8° from the center due to the loss in detection efficiency. The simulated data rates and optimized cuts agree well with the experimental results. Since the efficiency of the detector falls off above a radius of 0.8° , we only use the central 1.6° diameter region. If TeV emission mimics the thermal surface brightness, we would see almost all of the emission expected. Unfortunately, our search has only very limited sensitivity beyond the central 0.8° from the center of the field of view.

We then searched over the central 0.8° radius region of the field of view of the camera for point sources within the clusters. At

²¹ See <http://www.physics.utah.edu/gammaray/GriSU>.

TABLE 2

VALUES OF THE DOUBLE- β MODEL PARAMETERS FOR THE PERSEUS CLUSTER OF GALAXIES FROM PFOMMER & ENBLIN (2004) AND BASED ON DATA FROM CHURAZOV ET AL. (2003) AND STRUBLE & ROOD (1999)

Cluster	a_1	a_2	r_1 (kpc)	r_2 (kpc)	β_1	β_2
Perseus	1.0	0.104	57	200	1.2	0.58
Abell 2029	1.0	N/A	212	N/A	0.83	N/A

NOTE.—The values shown for Abell 2029 are for a King profile based on data from Jones & Forman (1984).

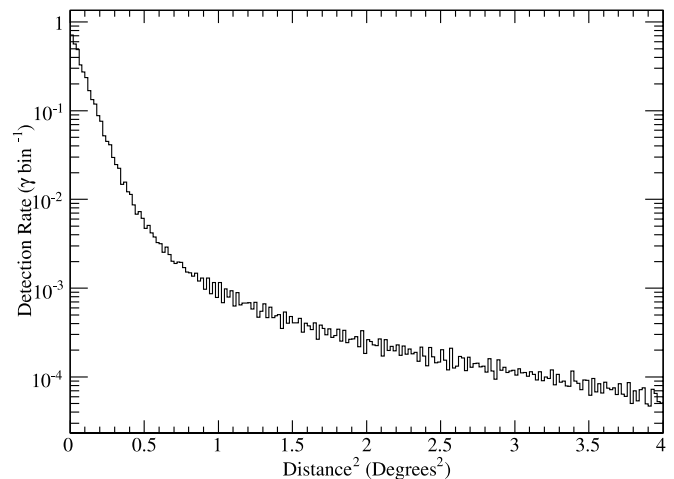
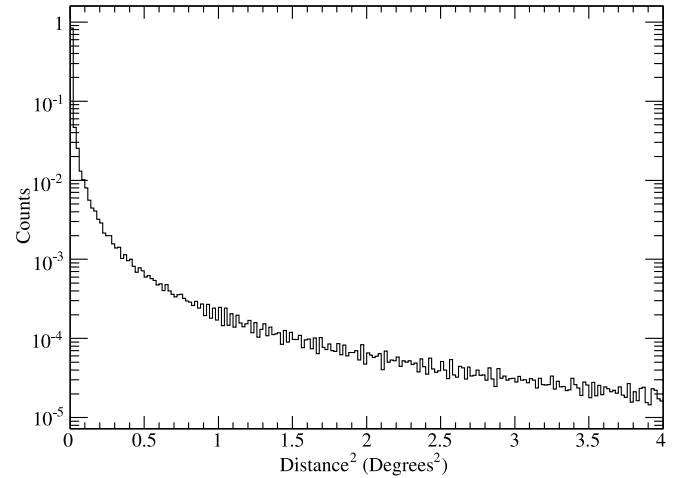


FIG. 5.—*Top*: Expected count distribution for the Whipple telescope based on the double- β profile for the Perseus Cluster (eq. [2]) normalized so that the area under the curve is 1.0. *Bottom*: Count distribution convolved with the angular resolution and the Crab detection rate of the Whipple 10 m telescope. The lower plot can be integrated to give the total expected signal from the Perseus Cluster if it shines with the flux of the Crab Nebula. A fact to note is that almost all the expected emission arises from within 0.3° of the cluster core.

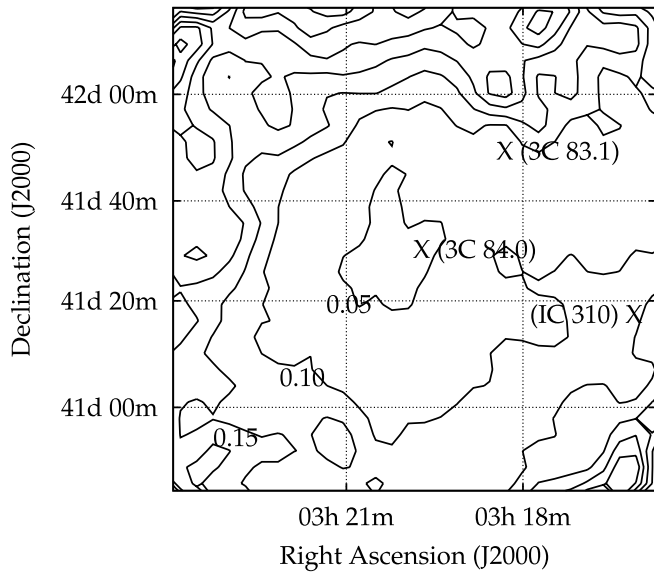


FIG. 6.—Gamma-ray flux upper limit map (90% confidence level) from point sources of the inner 1° of the Perseus Cluster of galaxies. The scale is in units of flux from the Crab Nebula with each contour step equal to 0.05 times the Crab flux. The approximate location of the radio sources found in Table 3 are shown.

every point in the field of view, we applied the optimal cut as specified and calculated the excess or deficit of candidate gamma rays from the data. We normalized the excess or deficit counts to the experimentally measured Crab rates from the same observing season. We then used this flux and its error to calculate a Bayesian upper limit on the flux (Helene 1983), taking into account the statistical error for the Crab event rate.

To search for extended emission from the Perseus Cluster, we assumed that the TeV gamma-ray surface brightness mimics that of the thermal X-ray emission seen by *Chandra* (Sanders et al. 2005) and *BeppoSAX* (Nevalainen et al. 2004), which arises from interactions of the thermal protons in the cluster. The X-ray surface brightness can be modeled as a double- β profile:

$$\Sigma(r) \propto \left[\sum_{i=1}^2 a_i \left(1 + \frac{r^2}{r_i^2} \right)^{-3\beta_i/2} \right]^2, \quad (2)$$

where $\Sigma(r)$ is the surface brightness and a_i , r_i , and β_i are isobaric model parameters (Pfrommer & Enßlin 2004). The values of these parameters, based on results from Churazov et al. (2003) and Struble & Rood (1999), can be found in Table 2. The emission will continue out to the accretion shock, which is expected to occur at $\sim 2.2^\circ$ from the cluster center. Assuming that the double- β profile, we estimate that our angular cut of 0.3° from

the cluster center optimizes the sensitivity of the search for cluster emission. A fraction of 95% of the total cluster emission comes from within 0.3° from the cluster. Figure 4 shows the ON and OFF data after analysis and cleaning plotted versus the distance from the center of the field of view squared. There is an excellent match between the ON and OFF data and no obvious excess out to the edge of the field of view.

The X-ray surface brightness is better modeled in the case of Abell 2029 by a single- β King profile (King 1972) given by

$$\Sigma(r) \propto a_i \left(1 + \frac{r^2}{r_i^2} \right)^{-3\beta_i+1/2}. \quad (3)$$

The model parameters are found in Table 2 and are from Jones & Forman (1984) based on observations made with the *Einstein* observatory. We chose the *Einstein* observations over more recent observations by *Chandra* due to the larger field of view of *Einstein*. For this cluster, the X-ray emission continues out to $\sim 1.0^\circ$ from the center of the cluster, and 96% of the emission comes from the central 0.3° .

We derived quantitative upper limits by normalizing these profiles over the field of view of the camera. We then convolved the expected emission by the point-spread function of the Whipple telescope, multiplied by the offset-dependent Crab detection rate. The method generates a map of the expected detection rate, assuming that the entire cluster produces the same TeV flux as the Crab Nebula. Figure 5 shows the expected emission based on the double- β profile for the Perseus Cluster at various stages in the analysis process. The rate map and actual excess were integrated over the inner 0.3° , and these two values were used to determine the upper limit on the diffuse TeV flux from the entire cluster in units of the Crab flux. We also computed upper limits by integrating counts over the most sensitive 0.8° region of the camera.

3. RESULTS

For the Perseus Cluster, Figure 4 shows that there is no excess detected in the field of view of the camera. Using a radial cut of 0.3° , our analysis results in a significance of -2.1 standard deviations and an upper limit on the diffuse emission of 13% of the Crab flux (7.4×10^{-12} ergs $\text{cm}^{-2} \text{s}^{-1}$). Figure 6 is a map of upper limits on the point source emission. All of the upper limits are below 0.45 crab, and most (80%) are below 0.05 crab. Table 3 lists the upper limits at the locations of the three radio galaxies associated with spectroscopically identified cluster galaxies. The upper limit on the TeV emission from the central galaxy, NGC 1275, is 4.0% of the Crab flux (2.7×10^{-12} ergs $\text{cm}^{-2} \text{s}^{-1}$).

Abell 2029 does not show any evidence for point source or extended emission. Figure 7 shows a map of upper limits on the point source emission. All of the upper limits are below 1.1 crab with the majority (80%) below 0.1 crab. Table 3 lists an upper

TABLE 3
GAMMA-RAY FLUX 90% UPPER LIMITS ON SPECTROSCOPICALLY RESOLVED RADIO GALAXIES ASSOCIATED WITH MEMBERS OF THE PERSEUS AND ABELL 2029 CLUSTERS OF GALAXIES

CLUSTER	SOURCE	R.A. (J2000.0)	DECL. (J2000.0)	20 cm FLUX (mJy)	400 GeV FLUX UPPER LIMIT	
					Crab	10^{-11} ergs $\text{cm}^{-2} \text{s}^{-1}$
Perseus	3C 84.0 (NGC 1275)	03 19 48	+41 30 42	2829.2	0.047	0.29
Perseus	3C 83.1 (NGC 1265)	03 18 16	+41 51 27	1305.5	0.086	0.53
Perseus	IC 310	03 16 43	+41 19 29	168.1	0.13	0.80
Abell 2029	IC 1101	15 10 56	+05 44 42	527.8	0.13	1.1

NOTE.—The 20 cm flux data are from The NRAO VLA Sky Survey (Condon et al. 1998).

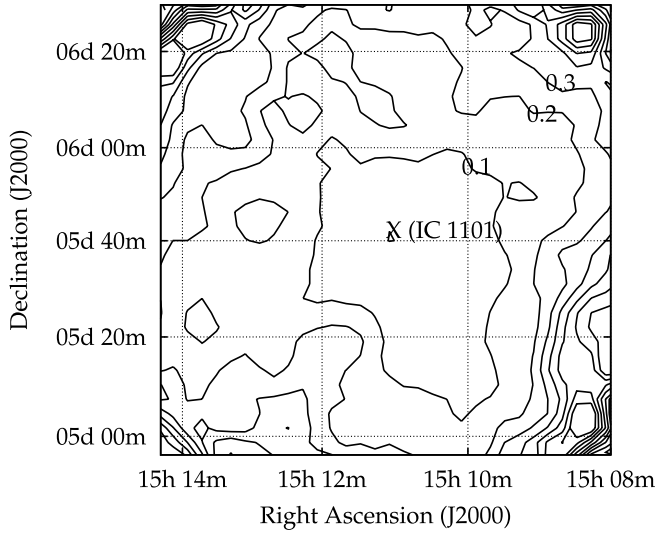


FIG. 7.—Gamma-ray flux upper limit map (90% confidence level) from point sources of the inner 1° of the Abell 2029 cluster of galaxies. The scale is in units of flux from the Crab Nebula with each contour step equal to 0.1 times the Crab flux. Select contours are labeled. The location of the central brightest radio galaxy is shown.

limit of 13% of the Crab flux (14×10^{-12} ergs cm^{-2} s^{-1}) for the central radio galaxy. Within 0.3 from the camera center, we find a deficit of 13 counts with a statistical significance of -0.15 standard deviations. Assuming the emission profile of Abell 2029 follows equation (3), we compute an upper limit on the diffuse emission of 14% of the Crab flux (16×10^{-12} ergs cm^{-2} s^{-1}). Table 4 gives a summary of the various upper limits for each cluster. All upper limits discussed in this paper have been computed for the gamma-ray emission from within 0.2 , 0.3 , and 0.8 angular distance from the cluster core. Flux upper limits have been scaled based on the assumed spectral shape after absorption.

4. INTERPRETATION AND DISCUSSION

Figure 8 shows our upper limits on TeV emission from the two clusters and compares them to previous upper limits from EGRET (Reimer et al. 2003), with the results of model calculations. The lines show models of the CRP-induced gamma-ray emission normalized to the EGRET upper limits, assuming a CRP spectrum with differential spectral index of -2.1 (Pfrommer & Enßlin 2004). This index is a reasonable choice of the source spectrum because galaxy clusters are not “leaky” and retain all

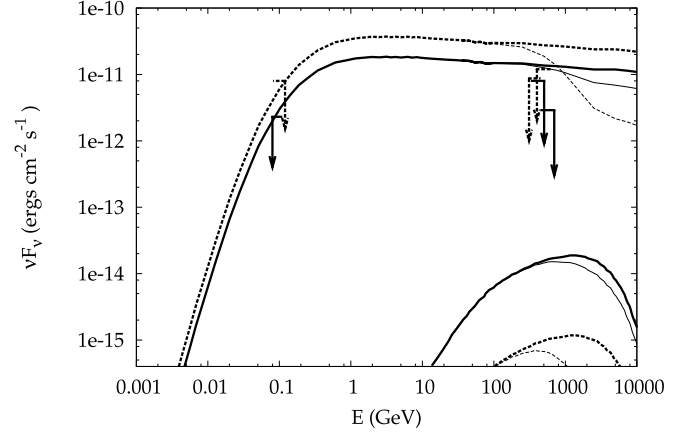


FIG. 8.—In this plot, the solid lines correspond to the Perseus Cluster and the dashed lines to Abell 2029. The Whipple 90% upper limits on the emission from the clusters are plotted at 400 GeV (offset to improve readability) with the higher values in each case corresponding to an angular cut of 0.3 (optimized for the search for diffuse CRP emission) and the lower to a cut of 0.2 (optimized for the search for point sources and dark matter). The upper solid and dashed lines show the CRP-induced pion decay gamma-ray emission (Pfrommer & Enßlin 2004) normalized to the EGRET 100 MeV upper limit (shown at 100 MeV). Also plotted (the lower flux emission at the bottom right) is the dark matter emission derived under the assumption that the TeV gamma-ray signal from the galactic center originates from the annihilation of an 18 TeV neutralino (Horns 2005), which should be compared to the point source upper limits (0.2 cut). The thin lines emanating from the pion and dark matter spectra show the effect of extragalactic extinction owing to pair production processes.

CRPs, unlike our Galaxy where leakage of high-energy CRPs is thought to steepen the source spectrum of -2.1 to the observed value of -2.7 . If we assume a spectral index of -2.3 , the Whipple and EGRET upper limits are equivalent. Also shown on this plot (as a thinner extension to the main lines) is a prediction of the emission modified by extragalactic extinction owing to pair production processes of TeV photons with photons of the cosmic infrared background ($\gamma_{\text{TeV}} + \gamma_{\text{CIB}} \rightarrow e^+ + e^-$). The extinction calculation assumes the phenomenological background model (“P0.45”) of Aharonian et al. (2005). Extragalactic extinction has only a minor impact on the flux predictions for Perseus owing to its low redshift. However, Abell 2029 is significantly farther away, and extinction does influence the observed spectrum, which we take into consideration when calculating upper limits. The Whipple upper limits (this paper) lie by factors of 4.6 (Perseus) and 4.2 (Abell 2029) below the model extrapolations. If the CRP spectrum indeed follows a power-law distribution with differential spectral index of -2.1 up to multi-TeV energies, the calculations

TABLE 4
UPPER LIMITS FOR THE DIFFUSE CRP EMISSION FROM PERSEUS AND ABELL 2029 USING VARIOUS ANGULAR CUTS

CLUSTER	ANGULAR CUT (deg)	SIGNIFICANCE (σ)	400 GeV FLUX UPPER LIMIT		
			Crab	10^{-11} ergs cm^{-2} s^{-1}	SCALING FACTOR
Perseus	0.2	-2.3	0.047	0.29	0.80
	0.3	-2.1	0.13	0.80	0.80
	0.8	-0.91	0.12	0.74	0.80
Abell 2029	0.2	-1.2	0.10	0.87	1.1
	0.3	-0.15	0.14	1.2	1.1
	0.8	-0.79	0.25	2.2	1.1

NOTES.—The 0.2 cut is relevant for point source and dark matter emission. The 0.3 cut is the optimal cut for the extended emission while the 0.8 one contains the emission from a large fraction of the field of view. The scaling factor is used to convert upper limits from Crab units to differential fluxes, taking into account the expected spectral shape.

of Pfrommer & Enßlin (2004) together with our results imply that the nonthermal CRP energy density is less than 7.9% of the thermal energy density for the Perseus Cluster.

The lower lines in Figure 8 show the expected emission from dark matter annihilations derived under the optimistic assumption that the TeV emission from the galactic center (Aharonian et al. 2004; Kosack et al. 2004; Tsuchiya et al. 2004; Horns 2005) originates entirely from such annihilations. We scale the gamma-ray flux from the galactic center by computing the expected annihilation signal for the Galactic center, the Perseus Cluster, and Abell 2029 from a Navarro-Frenk-White (NFW) halo (Bergström et al. 1998) with $\rho \propto [r/r_s(1 + r/r_s)^2]^{-1}$, virial radius $r_s \simeq 290$ kpc, a halo mass of 4×10^{14} , a distance of 75 Mpc, and an NFW concentration parameter of $c \simeq 4$. We find that the best sensitivity (signal-to-noise ratio) is obtained if we use the same radial cut, $\theta = 0.3$, as for the search for point sources (reducing background from misidentified CR air showers). The expected dark matter signal lies 2 orders of magnitude or more below our upper limits. We will not see dark matter emission even if all of the TeV galactic center emission is dark matter in origin. Thus, we do not provide any new constraints on TeV

galactic center emission. Second, our calculations show that the most promising region to observe dark matter is the galactic center.

Although we did not detect significant TeV gamma rays from these two clusters of galaxies, we are able to determine two different types of upper limits on the emission: from point sources within the cluster and upper limits on the extended emission. Long-duration observations with the more sensitive TeV telescopes VERITAS, HESS, MAGIC, and CANGAROO III, and the GeV telescope GLAST will be critical for determining whether cluster are emitters of high-energy gamma rays.

This research is supported by grants from the U.S. Department of Energy, the U.S. National Science Foundation, the Smithsonian Institution, by NSERC in Canada, by Science Foundation Ireland, and by PPARC in the UK. H. K. acknowledges the support of the DOE in the framework of the Outstanding Junior Investigator Award. J. S. P. acknowledges the support by the Dean of the Arts and Sciences Graduate School of Washington University in St. Louis through a dissertation fellowship. We would also like to thank Jonathan Katz for his comments and suggestions.

REFERENCES

- Aharonian, F., et al. 2004, *A&A*, 425, L13
 ———. 2005, *Nature*, submitted (astro-ph/0508073)
 Bergström, L., Ullio, P., & Buckley, J. H. 1998, *Astropart. Phys.*, 9, 137
 Blasi, P., & Colafrancesco, S. 1999, *Astropart. Phys.*, 12, 169
 Bowyer, S., & Berghöfer, T. W. 1998, *ApJ*, 506, 502
 Buckley, J. H., et al. 1998, *A&A*, 329, 639
 Churazov, E., Forman, W., Jones, C., & Böhringer, H. 2003, *ApJ*, 590, 225
 Colafrancesco, S. 2001, in *AIP Conf. Proc. 587, Gamma 2001: Gamma-Ray Astrophysics*, ed. S. Ritz, N. Gehrels, & C. R. Shrader (New York: AIP), 427
 Condon, J. J., Cotton, W. D., Greisen, E. W., Yin, Q. F., Perley, R. A., Taylor, G. B., & Broderick, J. J. 1998, *AJ*, 115, 1693
 Donahue, M. E., Voit, G. M., & Cavagnolo, K. 2004, *BAAS*, 205, 60.20
 Enßlin, T. A., & Biermann, P. L. 1998, *A&A*, 330, 90
 Fegan, S. J., et al. 2005, *ApJ*, 624, 638
 Feretti, L. 2003, in *Texas in Tuscany: 21st Symp. on Relativistic Astrophysics*, ed. R. Bandiera, R. Maiolino, & F. Mannucci (Singapore: World Scientific), 209
 Finley, J. P., et al. 2001, in *Proc. 27th Int. Cosmic Ray Conf. (Hamburg)*, 2827
 Fusco-Femiano, R., dal Fiume, D., Feretti, L., Giovannini, G., Grandi, P., Matt, G., Molendi, S., & Santangelo, A. 1999, *ApJ*, 513, L21
 Fusco-Femiano, R., Orlandini, M., Brunetti, G., Feretti, L., Giovannini, G., Grandi, P., & Setti, G. 2004, *ApJ*, 602, L73
 Giovannini, G., & Feretti, L. 2000, *NewA*, 5, 335
 Giovannini, G., Feretti, L., Venturi, T., Kim, K.-T., & Kronberg, P. P. 1993, *ApJ*, 406, 399
 Giovannini, G., Tordi, M., & Feretti, L. 1999, *NewA*, 4, 141
 Girardi, M., Giuricin, G., Mardirossian, F., Mezzetti, M., & Boschin, W. 1998, *ApJ*, 505, 74
 Helene, O. 1983, *Nucl. Instrum. Methods Phys. Res.*, 212, 319
 Hillas, A. M. 1985, in *Proc. 19th Int. Cosmic Ray Conf. (Leeds)*, 445
 Horns, D. 2005, *Phys. Lett. B*, 607, 225
 Jones, C., & Forman, W. 1984, *ApJ*, 276, 38
 Kang, H., & Jones, T. W. 2005, *ApJ*, 620, 44
 Kawasaki, W., & Totani, T. 2002, *ApJ*, 576, 679
 Kempner, J. C., & Sarazin, C. L. 2001, *ApJ*, 548, 639
 King, I. R. 1972, *ApJ*, 174, L123
 Kosack, K. 2005, Ph.D. thesis, Washington Univ. in St. Louis
 Kosack, K., et al. 2004, *ApJ*, 608, L97
 Krawczynski, H. 2002, *ApJ*, 569, L27
 Lieu, R., Ip, W.-H., Axford, W. I., & Bonamente, M. 1999, *ApJ*, 510, L25
 Lieu, R., Mittaz, J. P. D., Bowyer, S., Breen, J. O., Lockman, F. J., Murphy, E. M., & Hwang, C.-Y. 1996, *Science*, 274, 1335
 Markevitch, M., Forman, W. R., Sarazin, C. L., & Vikhlinin, A. 1998, *ApJ*, 503, 77
 Nevalainen, J., Oosterbroek, T., Bonamente, M., & Colafrancesco, S. 2004, *ApJ*, 608, 166
 Pfrommer, C., & Enßlin, T. A. 2004, *A&A*, 413, 17
 Punch, M., & Fegan, D. J. 1991, in *AIP Conf. Proc. 220, High Energy Gamma-Ray Astronomy*, ed. J. Matthews (New York: AIP), 321
 Reimer, O., Pohl, M., Sreekumar, P., & Mattox, J. R. 2003, *ApJ*, 588, 155
 Rephaeli, Y. 1977, *ApJ*, 218, 323
 Rephaeli, Y., Gruber, D., & Blanco, P. 1999, *ApJ*, 511, L21
 Reynolds, P. T., et al. 1993, *ApJ*, 404, 206
 Ryu, D., Kang, H., Hallman, E., & Jones, T. W. 2003, *ApJ*, 593, 599
 Sanders, J. S., Fabian, A. C., & Dunn, R. J. H. 2005, *MNRAS*, 360, 133
 Scharf, C. A., & Mukherjee, R. 2002, *ApJ*, 580, 154
 Struble, M. F., & Rood, H. J. 1999, *ApJS*, 125, 35
 Tsuchiya, K., et al. 2004, *ApJ*, 606, L115
 Völk, H. J., & Atoyan, A. M. 1999, *Astropart. Phys.*, 11, 73
 Weekes, T. C. 1996, *Space Sci. Rev.*, 75, 1